# Sacrificial Powder Pressure Control for Infiltration of Microscale Metal Parts

Henry Dean Davis

A capstone report submitted to the faculty of

Brigham Young University

In partial fulfillment of the requirements for the degree of

Bachelor of Science

Richard Vanfleet, Advisor

Department of Physics and Astronomy

Brigham Young University

April 13, 2022

Copyright © 2022 Henry Dean Davis

All Rights Reserved

# ABSTRACT

Sacrificial Powder Pressure Control for Infiltration of Microscale Metal Parts

Henry Dean Davis

Department of Physics and Astronomy

Bachelor of Science

Microchannels were fabricated using stainless-steel binder jetting and bronze infiltration. In this approach, infiltrant must fill the porous printed material without filling the microchannels. This was achieved through a high-yield fabrication method called sacrificial powder infiltration (SPI). In SPI, sacrificial powder reservoirs (pore size ~60 µm) are used to control infiltrant pressure, causing infiltrant to selectively fill the small pores between particles in the printed part (pore size ~3 µm) while leaving the microchannels (700, 930 µm) empty. To develop the SPI method, a pore filling study was performed in this stainless-steel/bronze system with 370 µm, 650 µm, and 930 µm microchannel segments; this study informed adjustments to the capillary model of infiltration when used to guide SPI design.

Keywords: Microfluidics; Microchannels; Binder-Jet Printing; Pressure Control; Infiltration

# Contents

ABSTRACT ..... 3
Acknowledgments ..... 23
1. Introduction ..... 5
2. Materials and Methods ..... 7
2.1 Printing ..... 7
2.2 Sintering ..... 7
2.3 Infiltration: Pore Filling Study ..... 8
2.4 Infiltration: Sacrificial Powder Study ..... 9
3. Theory: Capillary Model and Infiltrant Pressure ..... 9
4. Results and Discussion ..... 12
4.1 Pore Filling Study Results ..... 13
4.2 Pore Filling Study Discussion ..... 15
4.2.1 Infiltrant Height Deviation from Average: ..... 15
4.2.2 Average Height Difference Between Different Sized Holes: ..... 16
4.2.3 Applying the Capillary Model of Infiltration to SPI Design ..... 17
4.3 Sacrificial Powder Infiltration Study Results ..... 17
4.4 Sacrificial Powder Infiltration Study Discussion ..... 19
5. Conclusion ..... 20
References ..... 21
Supplementary Material ..... 23
Furnace Setup: ..... 24
Additional Samples from Pore Filling Study: ..... 24

# 1. Introduction

The ability to create high resolution complex structures has enabled additive manufacturing (AM) to revolutionize some microfabrication processes with applications ranging from micro robotics to multilayer printed circuits (Goh et al., 2021; Li and Pumera, 2021; Sirringhaus et al., 2000; Zhu et al., 2015). Recent efforts have enabled the use of AM in microfluidic applications by using polymer AM to create complex microchannels. (Nielsen et al., 2020; Rogers et al., 2015). Traditionally, microfluidic devices have been fabricated using cleanroom lithography and etching or molding fabrication processes which allow for precise microscale features but are compatible with few materials and lack the ability to form complex 3D designs. The flexibility of AM has allowed various 3D microfluidic structures to be formed, including active components such as integrated valves and pumps (Gong et al., 2016). Some microfluidic applications like micro heat exchangers or microcolumns for gas chromatography could benefit from the design flexibility inherent in additive manufacturing (Dahmen et al., 2020), but call for high temperatures and high thermal conductivity (Ghosh et al., 2018). Laser powder bed fusion (LPBF) is one method that has been used to form metal microchannels for microfluidic applications (Gupta et al., 2016; Phyo et al., 2020)

A promising candidate for fabrication of fluidic microchannels in high temperature, high thermal conductivity material is metal binder-jetting (BJ), a parallel AM process capable of high throughput manufacturing (Sachs et al., 1990; Ziaee and Crane, 2019). However, metal BJ printed parts are composed of a porous printed matrix that must be sealed; this can be done using high temperature sintering or metal infiltration. Sachs et al. used bronze infiltration to seal the porous printed matrix (pore size ~20 μm) of a stainless-steel (SS) part while leaving channels (1-3 mm diameter) free of infiltrant (Sachs et al., 2000). To do this they recognized that infiltration

preferentially fills smaller pores over larger pores and used gravitational pressure control to fill the porous printed matrix while preventing the channels from filling. Extending BJ printing and infiltration to the formation of sub-millimeter scale fluidic channels requires better understanding of infiltrant pressure in these systems. Also needed are new methods for pressure control that will provide lower infiltrant pressure which is required to keep microscale channels clear of infiltrant.

Here we present a method for sealing the porosity in BJ printed parts with sub-millimeter scale internal structures; we call this method sacrificial powder infiltration (SPI). In SPI, after printing and sintering of a part but prior to bronze infiltration, a reservoir of sacrificial powder is placed in contact with the part. This sacrificial powder has pore dimensions larger than the pores in the porous printed matrix but smaller than the microchannels (figure 1 a-c). Therefore, after the porous printed matrix fills with infiltrant, excess infiltrant fills the sacrificial powder instead of the microchannels (figure 1 d, e). SPI provides the lower pressures needed for infiltrating BJ parts with microscale channels. SPI also enables local pressure control, reducing the impact of pressure variations across a part.

To aid in understanding infiltration of microscale features in this SS/bronze system, we performed a pore filling study. In this study, we analyzed pore filling in microchannel segments with diameters of 370 μm, 650 μm, and 930 μm. Based on the results of this study, we show that adjustments to the capillary model of infiltration are needed for accurate predictions in the SS/bronze system. Lastly, drawing on these adjustments to inform design, we used SPI to fabricate 37 mm long, 700 μm and 930 μm diameter microchannels.

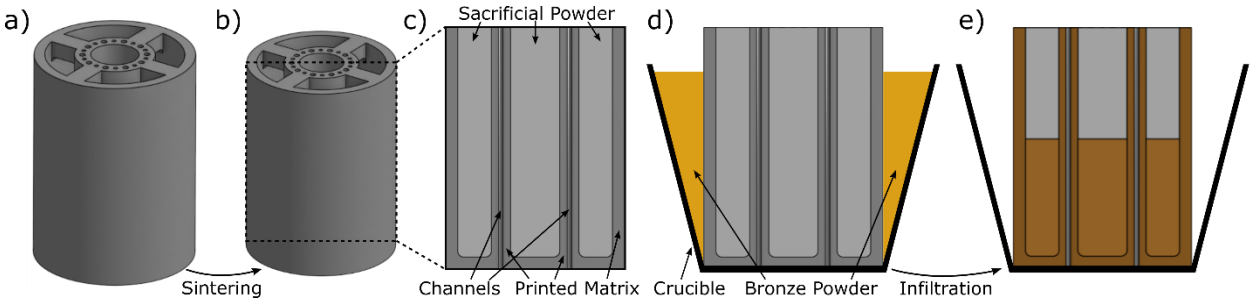



*Figure 1: Sacrificial powder infiltration process: a) a printed part b) a sintered part showing some shrinkage c) cross-section of a part showing two channels and the sacrificial powder reservoir d) a part in a crucible with bronze powder placed around it e) an infiltrated part showing filled printed matrix, partially filled sacrificial powder, and empty channels.*

## 2. Materials and Methods

### 2.1 Printing

An ExOne Innovent+ BJ printer was used to print SS samples. The powder used was gas atomized spherical SS316L powder with D90< 22 µm (ExOne Co.). ExOne aqueous binder (part #: 7100037CL) was used during printing and binder was cured by placing samples in an oven at 180°C for at least 6 hours. After curing, samples were removed from the print bed and loose powder was removed from semi-enclosed features using brushes and compressed air at 25-55PSI. As the channels were longer in the SPI study samples than other samples, sonication was also used for powder removal during which a small wire was inserted into the channels to loosen powder.

### 2.2 Sintering

Samples were sintered in a 2.7-inch tube furnace that included a heating zone and a cooling zone. For sintering, samples were placed into a SS sample holder and pushed into the heating zone. Argon and hydrogen were then flowed through the tube at 700 SCCM and 200 SCCM, respectively, while the temperature was ramped from room temperature to ~800°C (ramp

rate ~13°C/min), held for 1 hour for binder burnout, ramped to the desired sintering temperature (ramp rate ~6°C/min), and held for 20 min. Samples were cooled rapidly as follows. For the last 5 min of the sintering time, hydrogen flow was stopped and argon flow was increased to 1400 SCCM to flush the hydrogen from the tube. After this, the sample was rapidly moved to the cooling zone (~200°C), left there for 20 min. under the argon flow, and then removed from the furnace.

## 2.3 Infiltration: Pore Filling Study

After sintering, samples were infiltrated with bronze using -325 mesh 10% Sn bronze powder (OzoMetal LLC) as follows. The needed amount of bronze infiltrant depended on the post-sintering void fraction of the porous printed matrix and was calculated according to Eq. 1:

$$M_{bronze} = \left(\frac{M * V_{design} * shrink}{M_{avg}} - \frac{M}{\rho_{SS}} + V_{channels} * shrink\right) * \beta * Fill_{target} * \rho_{bronze} \qquad (1)$$

where the terms within the parentheses give the total void volume of the part and are from left to right: the total volume of the pores in the printed part, the volume occupied by SS, the volume of the channels. The terms in the equation are as follows: *M* is the post-sintering measured mass of the individual sample, $M_{avg}$ is the average post-sintering mass of samples, shrink is the fractional volumetric shrinkage due to sintering (calculated by measuring part dimensions before and after sintering), $\rho_{SS}$ is the density of bulk SS316L, $V_{channels}$ is the total designed volume of the channels, $\beta$ is the volumetric thermal expansion of stainless steel at 1000°C which affects the void volume of the part (~1.05), $Fill_{target}$ is the desired fractional fill of the total void volume, and $\rho_{bronze}$ is the estimated density of liquid bronze (~8.15 g/cm$^3$). The bronze was placed into an infiltrant holder printed as part of the sample. Samples were placed into a quartz lined SS sample holder and put into the furnace by initially setting the sample inside the cooling zone, closing the end cap, and flowing argon at 1400 SCCM for 5 min to flush air from the tube. The

sample was then moved to the heating zone (~800°C), argon and hydrogen flow were set to 700 SCCM and 200 SCCM, respectively, and the furnace was ramped to the infiltration temperature where it was held for the desired infiltration time (ramp rate ~6°C/min). Samples were then cooled according to the same rapid cooling procedure used after sintering. After removal from the furnace, the through-hole plate was optically imaged (while backlit with a white LCD screen) to determine which holes were empty and fill height was measured as the height of the highest filled hole in each column.

### 2.4 Infiltration: Sacrificial Powder Study

For the sacrificial powder study, samples were infiltrated using the same process as the pore filling study with a few differences. Prior to infiltration, sacrificial powder was poured into the sacrificial powder cavities (see figure 1c). Sacrificial powder was water atomized -100 mesh (particle diameter <150 µm) SS316L powder (Thermo Fisher Scientific, product #: 11089). Sacrificial powder mass and volume were measured to calculate a void fraction of ~58%. Samples were placed into an alumina crucible and bronze powder was placed in the crucible around the sample. Following infiltration, channel filling was checked using backlighting and samples were milled for optical imaging.

## 3. Theory: Capillary Model and Infiltrant Pressure

The capillary model of infiltration predicts that small pores will preferentially fill over large pores and that pore filling is determined by capillary pressure ($P_c$). We define $P_c$ as the pressure in the infiltrant of a partially filled pore relative to the adjacent gas. $P_c$ is negative and governed by the following equation:

$$P_c = \frac{-4\sigma Cos(\theta)}{D} \quad (2)$$

where $\sigma$ is the infiltrant surface tension, $\theta$ is the contact angle, and $D$ is the diameter of a long cylindrical pore (Fanchi, 2002). For the non-cylindrical pores in a spherical powder, the relationship between powder particle diameter and $P_c$ of the interstitial pores was found (following Dodds and Srivastava, 2006) to be:

$$P_c = \frac{-6\sigma}{D_{sv}} \frac{(1-\varepsilon)}{\varepsilon} \tag{3}$$

where $\varepsilon$ is the porosity of the powder and $D_{sv}$ is the mean surface volume particle diameter.

During infiltration, the capillary model predicts that pores with capillary pressure below (more negative than) the infiltrant pressure will fill and pores with capillary pressure above the infiltrant pressure will remain empty. Without external control, pores will fill until all infiltrant is used up, with the final infiltrant pressure being determined by the smallest partially filled pore. One could imagine infiltrating a part with the exact amount of infiltrant needed to fill the porous printed matrix while leaving channels empty. However, in practice uncertainties in total pore volume mean that this approach would inevitably lead to either some unfilled pores in the printed matrix or some filled channels (fig 2a). Infiltrant pressure control can be used to overcome this shortcoming. Sachs et al. used gravimetric pressure control (Sachs et al., 2000) in which infiltrant pressure is controlled by fixing the height of the part above an infiltrant reservoir so that, as illustrated in fig. 2b., the infiltrant pressure is reliably above that needed to fill the porous printed matrix but below that needed to fill the microchannels. Here we present an alternate method where infiltrant pressure is controlled by the size of pores in a sacrificial powder reservoir (as illustrated in fig 2b, 2c).

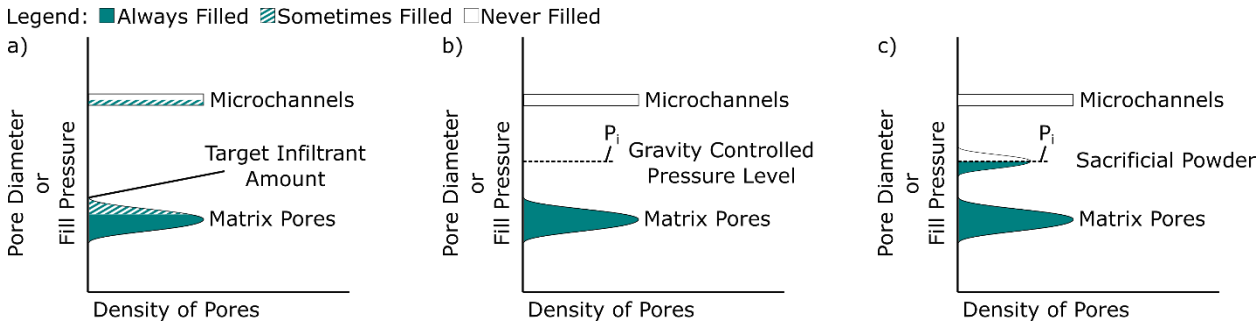



*Figure 2: Diagrams showing predicted fill levels in infiltrated samples: a) A sample without pressure control showing the potential for either an incompletely filled printed matrix or partially filled channels. b) A sample depicting gravity controlled infiltrant pressure. c) A sample depicting the pinning of the infiltrant pressure using a sacrificial powder.*

One advantage of using sacrificial pores to control infiltrant pressure rather than gravity is that sacrificial pores can more practically be used to keep small structures (such as microchannels) from filling. For example, a 250 µm channel is predicted to fill with infiltrant unless the infiltrant pressure is below -16 kPa (eq. 2), which would require a height of ~21 cm using gravimetric pressure control (calculated using $\Delta P=\rho g h$, where $\rho$ is the infiltrant density and $g$ is the gravitational constant), making it less practical due to furnace size limitations and infiltrant transport challenges. However, a sacrificial powder reservoir with an effective pore diameter smaller than 250 µm (powder diameter <500 µm) will achieve these infiltrant pressures.

For the pore filling study, it is valuable to understand how the capillary pressure and fill height (maximum height of filled pores) compare in pores of different sizes. The difference in capillary pressure between two different diameter pores $D_1$ and $D_2$ can be derived using eq. 2, resulting in:

$$\Delta P_c = 4\sigma Cos(\theta)\left(\frac{1}{D_2} - \frac{1}{D_1}\right) \quad (3)$$

The infiltrant pressure $P_i$ also varies with height according to $\Delta P_i = \rho g h$. By modifying Eq 3, we can find the expected difference in fill height between two pores:

$$\Delta h = \frac{4\sigma Cos(\theta)}{\rho g}\left(\frac{1}{D_2} - \frac{1}{D_1}\right) \quad (4)$$

Pressure equilibrium across a part predicts uniform fill-heights for channels of the same diameter and specific differences in fill height between channels of different diameter. We will compare the predictions of eq. 4 with experimental data in the next section.

## 4. Results and Discussion

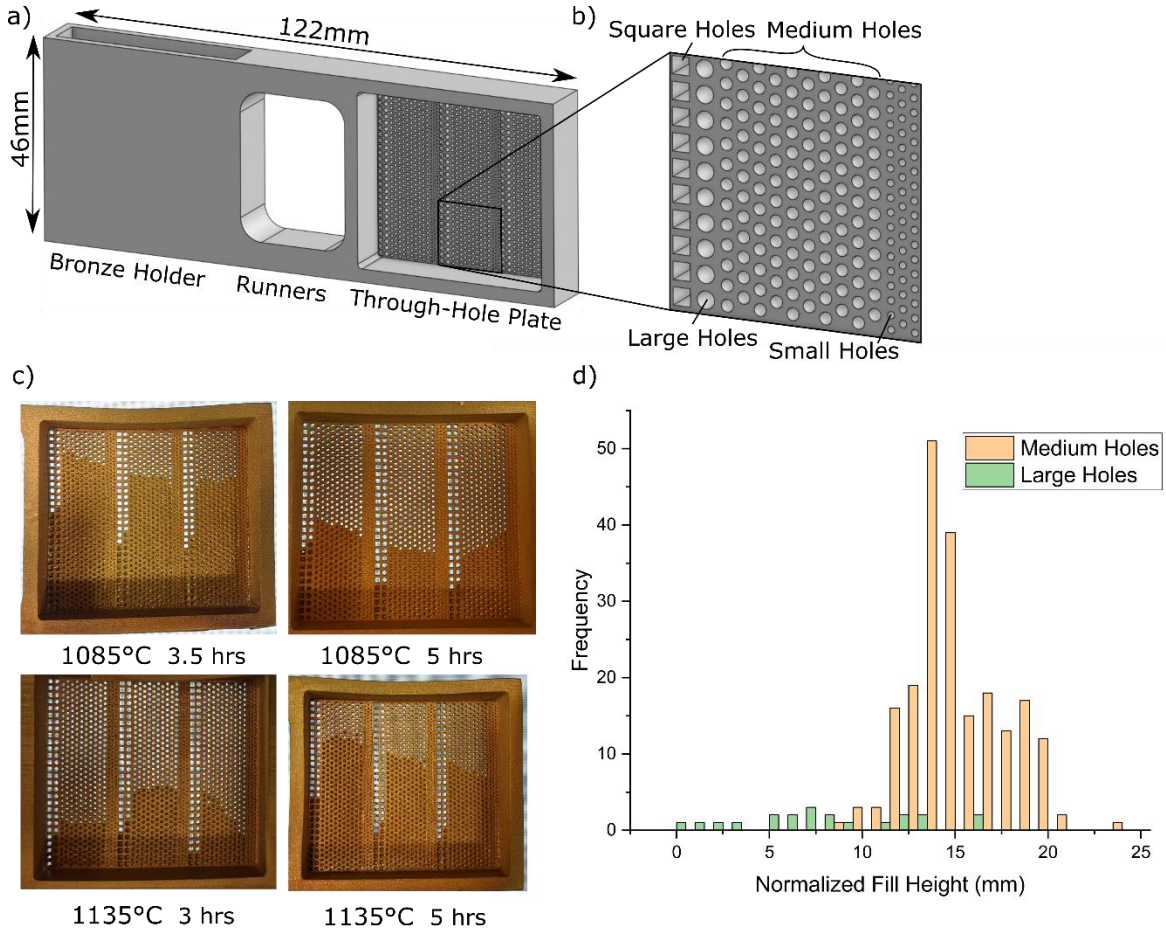


*Figure 3: Pore filling study: sample design and experimental results. a) CAD rendering of samples used in the pore filling study including a holder for bronze powder, two runners, and through-holes in a thin plate. b) A close-up view of the through-hole plate showing 2 mm length through-holes of varying sizes: square holes with dimensions 0.93x0.93 mm^2 and cylindrical holes with diameters of 0.93 mm (large), 0.65 mm (medium), and 0.37 mm (small). c) Optical transmission images of four samples after infiltration. d) Histogram of fill heights in each column of medium and large round holes normalized to the average fill height of medium hole columns in the sample.*

## 4.1 Pore Filling Study Results

To determine the dependence of pore filling on pore size, a pore filling study was conducted in samples with three different pore sizes and results were compared with capillary model predictions. Samples were designed with through holes (horizontal microchannel segments) to allow easy observation of pore filling as illustrated in figure 3(a and b). These through-hole samples were printed, sintered, and infiltrated. Various infiltration conditions (shown in table 1) were used to explore the effect of infiltration time and temperature on pore filling. Enough bronze powder was added to the bronze holder to allow filling of the porous printed matrix and roughly half of the through holes.

Table 1: Infiltration Times and Temperatures

| | Sintering | Infiltration |
|---|---|---|
| Condition 1 | 20 min at 1085C | 3.5 hrs at 1085C |
| Condition 2 | 20 min at 1085C | 5 hrs at 1085C |

| | | |
|---|---|---|
| Condition 3 | 20 min at 1135C | 3 hrs at 1135C |
| Condition 4 | 20 min at 1135C | 5 hrs at 1135C |

Optical transmission images of four infiltrated samples are shown in figure 3c (eight additional samples are shown in the supplementary material). There are several observations from these results:

1. The fill height of columns of smaller holes was generally greater than that of larger holes.
2. In same-sized holes, there was significant variation in column fill height across the sample. This lateral variation is well visualized in the medium hole columns where fill height can go up and down gradually across the sample.
3. There are abrupt fill height changes between adjacent columns with different sized holes. These abrupt changes are very different than the gradual changes in same sized holes mentioned above.
4. In almost all columns, holes are filled from the bottom up the with no empty holes below the highest filled holes. Across the 12 samples, the small hole columns almost always completely filled to the top of the sample (completely filled in 99 of 108 columns).

Observations 1, 3, and 4 are qualitative and in good agreement with capillary model predictions. The variation described in observation 2 represents a significant deviation from the model.

To quantify the variation in fill height of same-sized holes, statistical analysis was performed on the fill heights of medium and large round hole columns and shown in the histograms of Fig 3d. Medium hole columns show fill-height distributions which have standard

deviations and standard errors of 2.4 mm and 0.17 mm respectively. Large hole columns show fill-height distributions which have standard deviations and standard errors of 4.5 mm and 0.70 mm respectively. Empty small hole data is too sparse in these samples for statistical analysis. There was no clear dependence of pore filling on infiltration time or temperature, therefore all four infiltration conditions were lumped together for this statistical analysis. In 5 of the 12 samples, either the medium holes were completely filled or the large holes were completely empty; these cases did not allow for analysis of variation in fill heights and therefore were not included in the statistical analysis.

Two other quantitative findings of note are as follows: 1) the average difference in fill height between medium and large hole columns is 8.3 mm and 2) the expected fill level in the parts was predicted based on calculated void volume and infiltrant mass and compared with the measured fill level showing an uncertainty in the void volume of $\pm$10%.

## 4.2 Pore Filling Study Discussion

### 4.2.1 Infiltrant Height Deviation from Average:

The capillary model of infiltration suggests that at equilibrium, holes of the same diameter will fill with infiltrant to the same height. However, the range of fill heights in both the medium and large hole columns shows significant deviation from the average fill height. In extreme cases, this deviation can lead to large hole columns in some parts of the sample filling to greater heights than medium hole columns in other parts of the sample. This deviation in fill height happens quite gradually across the sample and, therefore, the greatest variation in fill height is seen when holes are separated by large lateral distances. We hypothesize that these variations are in large part due to temperature gradients during the rapid cooling process which drive infiltrant transport.

These deviations in the fill heights of the medium holes inform us about deviations in what we will call "effective pressure" across printed parts. Using the equation $\Delta P = \rho g \Delta h$ to convert the standard deviation from fill height gives an effective pressure deviation of 180 Pa across the part. We use the term effective pressure to recognize that while there are mechanisms other than pressure that could give rise to height deviations, converting height deviations to pressure allows us to compare them with capillary pressures. Capillary pressure as described in the theory section and referred to in Eq. 2, is the infiltrant pressure above which a pore will fill.

### 4.2.2 Average Height Difference Between Different Sized Holes:

The predicted difference in fill height between medium holes and large holes was 24 mm based on the capillary model. This prediction was made using Eq. 4 assuming zero contact angle, a literature value for the surface tension (Lee et al., 2004), and an estimated value of 7.85 g/cm$^3$ for the density of liquid bronze at 1000°C. Our observations, however, showed an average difference in fill height of only 8.3 mm between these hole sizes as seen in figure 3d. This discrepancy is much larger than the standard errors calculated from these measurements (0.17 mm and 0.70 mm for medium and large holes, respectively), indicating a significant quantitative difference between the model prediction and the results. We know that SS is dissolved into the bronze during infiltration. We could find no published values of surface tension for SS saturated bronze, but surface tension can be strongly dependent on composition: the addition of just 10% tin to copper reduces the surface tension of the alloy by a factor of 2 (Lee et al., 2004). Therefore, the surface tension used for our model predictions may not match our infiltrant. Another potential source of the discrepancy is that model predictions assumed long vertical channels, while our channel segments were both horizontal and short (diameter to length aspect ratios of 1:2 and 1:3).

### 4.2.3 Applying the Capillary Model of Infiltration to SPI Design

The discrepancies between model predictions and the results discussed in 4.2.1 and 4.2.2 suggest that adjustments to the capillary model of infiltration are needed for accurate predictions in the SS/bronze infiltration system. We will account for these non-idealities as follows: 1) we include a standard deviation in infiltrant pressure of 180 Pa to account for the variation in effective pressure, 2) we scale down capillary pressures for all pore sizes by a factor of 3 to account for surface tension uncertainty or other factors that could affect capillary pressure, and 3) we include an uncertainty in total void volume of ±10%. For high yield fabrication using SPI, the microchannels, the sacrificial powder, and the porous printed matrix must have capillary pressures that are different enough to account for these model adjustments.

## 4.3 Sacrificial Powder Infiltration Study Results

Based on the adjustments in 4.2.3, a study was done to test SPI fabrication of microchannels. Three samples were designed as shown in Fig. 1 (also 4a), printed, sintered (20 min at 1135°C), and infiltrated (3 hours at 1135°C). Samples were infiltrated with enough bronze to both fill the porous printed matrix and partially fill the sacrificial powder reservoirs. Capillary pressures for the porous printed matrix, the sacrificial powder, and the channel were calculated using Eq. 2 and Eq. 3 and are shown in Table 2. To ensure high-yield fabrication, the particle diameter of the sacrificial powder was chosen so that the differences in calculated capillary pressures between the three pore types in Table 2 were much larger than the variation in effective infiltrant pressure, even accounting for the scaling down of capillary pressures. The void volume of the sacrificial powder reservoirs was chosen to be approximately 40% of the total void volume to manage void volume uncertainty. Additionally, sacrificial powder was placed in close proximity with the channels to reduce the impact of infiltrant pressure variation across the part.

Table 2: Theoretical Capillary Pressures

| | $D_{sv}$ | $P_c$ (Unscaled) | $P_c$ (Scaled down by 3) |
|---|---|---|---|
| Porous Printed Matrix | 8.7 µm | -1200 kPa (Eq. 3) | -400 kPa |
| Sacrificial Powder | 70 µm | -61 kPa (Eq. 3) | -20 kPa |
| 700 µm Channel | N/A | -5.6 kPa (Eq. 2) | -1.9 kPa |

Calculations for Table 2 were performed as follows. The capillary pressure Pc of the channel was calculated using Eq. 2 with a channel diameter of 700 µm. Pc for the sacrificial powder and the porous printed matrix was calculated using Eq. 3 with porosities ε of .58 and .36, respectively, and mean surface volume particle diameters $D_{sv}$ of 70 µm and 8.3 µm, respectively, where $D_{sv}$ was determined by assuming spherical powder with normal distributions (having standard deviation 1/3 the average diameter) around averages of 80 µm and 10 µm for the sacrificial powder and the porous printed matrix, respectively.

Post infiltration analysis showed that in each sample: 1) the porous printed matrix was filled, 2) the sacrificial powder reservoir was partially filled, and 3) none of the 700 or 930 µm channels were filled. The optical image in Fig. 4b is from a region of an infiltrated sample and shows the well filled printed matrix, the partially filled sacrificial powder reservoirs, and an unfilled 700 µm channel.

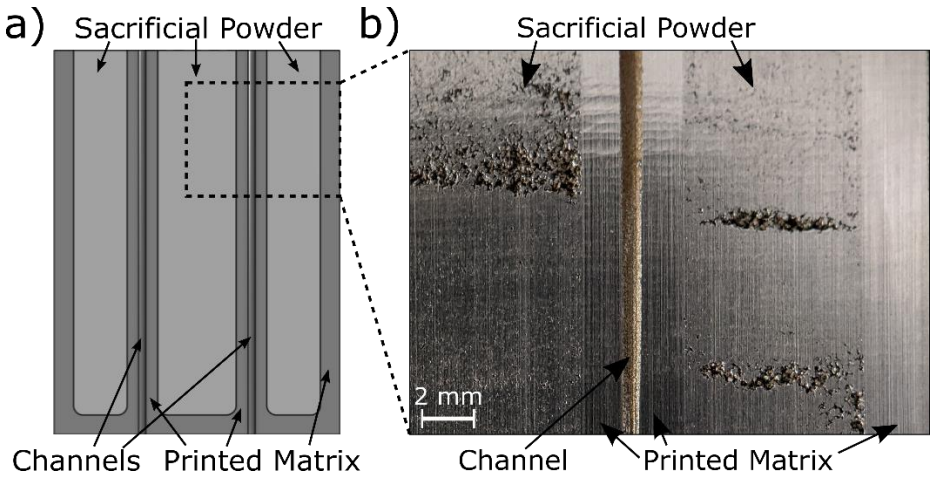



*Figure 4: Sacrificial powder infiltration: design tolerances and experimental results a) Section view of the cad file showing the porous printed matrix, the sacrificial powder placement, and exposed vertical channels. b) Image of a milled sample post-infiltration showing fully dense printed matrix, semi-porous sacrificial powder, and an unfilled 700* μm *channel.*

## 4.4 Sacrificial Powder Infiltration Study Discussion

In this study, twenty microchannels were successfully fabricated in each of three samples. These results show that SPI can be used for high-yield fabrication of metal microchannels, as predicted by the large differences between capillary pressures for each of the different pore types. Additionally, we believe that fabrication was successful because the sacrificial powder pores accounted for a large fraction of the total void volume and because the sacrificial powder was in close proximity to the channels. This work shows that with a few adjustments, the capillary model of infiltration is a useful tool for SPI fabrication design.

When using SPI for fabrication of parts with internal structures of different sizes than the channels fabricated here, the size of the sacrificial powder should be adjusted to ensure a large gap in capillary pressure is maintained between the different pore types. Additionally, if desired, sacrificial powder may be cut off after fabrication.

## 5. Conclusion

This work advances additive manufacturing of metal microfluidic devices by contributing sacrificial powder infiltration (SPI), a new method for infiltrant pressure control, and using this method to form sealed metal microchannels. SPI was used to seal the porous printed matrix of binder-jet printed parts while keeping printed microchannels free of infiltrant.

A better understanding of pore filling during infiltration was required in order to achieve high yields with the SPI process. Therefore, we analyzed pore filling in capillary segments with various diameters and found that while pore filling generally followed predictions from a capillary model of infiltration, there were significant deviations from the predicted behavior. Channels of a certain size did not always fill to the same height and the difference in fill height between channels of different sizes was much smaller than predicted. Based on these observations, we proposed adjustments to be accounted for when using the capillary model of infiltration to guide SPI design.

Lastly, we used SPI to fabricate 700 um and 930 um metal microchannels. Cross-sections of the parts show fully dense printed matrix, semi-porous sacrificial powder, and empty microchannels. The large difference in capillary pressure for these three structures enabled high-yield fabrication.

## References


Dahmen, T., Klingaa, C.G., Baier-Stegmaier, S., Lapina, A., Pedersen, D.B., Hattel, J.H., 2020. Characterization of channels made by laser powder bed fusion and binder jetting using X-ray CT and image analysis. Addit. Manuf. 36, 101445. https://doi.org/10.1016/j.addma.2020.101445

Dodds, J.A., Srivastava, P., 2006. Capillary Pressure Curves of Sphere Packings: Correlation of Experimental Results and Comparison with Predictions from a Network Model of Pore Space. Part. Part. Syst. Charact. 23, 29–39. https://doi.org/10.1002/ppsc.200501017

Fanchi, J.R., 2002. Measures of Rock-Fluid Interactions, in: Shared Earth Modeling. Elsevier, pp. 108–132. https://doi.org/10.1016/B978-075067522-2/50007-0

Ghosh, A., Vilorio, C.R., Hawkins, A.R., Lee, M.L., 2018. Microchip gas chromatography columns, interfacing and performance. Talanta. https://doi.org/10.1016/j.talanta.2018.04.088

Goh, G.L., Zhang, H., Chong, T.H., Yeong, W.Y., 2021. 3D Printing of Multilayered and Multimaterial Electronics: A Review. Adv. Electron. Mater. 7, 2100445. https://doi.org/10.1002/aelm.202100445

Gong, H., Woolley, A.T., Nordin, G.P., 2016. High density 3D printed microfluidic valves, pumps, and multiplexers. Lab. Chip 16, 2450–2458. https://doi.org/10.1039/C6LC00565A

Gupta, V., Talebi, M., Deverell, J., Sandron, S., Nesterenko, P.N., Heery, B., Thompson, F., Beirne, S., Wallace, G.G., Paull, B., 2016. 3D printed titanium micro-bore columns containing polymer monoliths for reversed-phase liquid chromatography. Anal. Chim. Acta 910, 84–94. https://doi.org/10.1016/j.aca.2016.01.012

Lee, J., Shimoda, W., Tanaka, T., 2004. Surface tension and its temperature coefficient of liquid Sn-X (X=Ag, Cu) alloys. Mater. Trans. 45, 2864–2870. https://doi.org/10.2320/matertrans.45.2864

Li, J., Pumera, M., 2021. 3D printing of functional microrobots. Chem. Soc. Rev. 50, 2794–2838. https://doi.org/10.1039/D0CS01062F

Nielsen, A.V., Beauchamp, M.J., Nordin, G.P., Woolley, A.T., 2020. 3D Printed Microfluidics 23.

Phyo, S., Choi, Sung, Jang, J., Choi, Sun, Lee, J., 2020. A 3D-printed metal column for micro gas chromatography. Lab. Chip 20, 3435–3444. https://doi.org/10.1039/D0LC00540A

Rogers, C.I., Qaderi, K., Woolley, A.T., Nordin, G.P., 2015. 3D printed microfluidic devices with integrated valves. Biomicrofluidics 9, 016501. https://doi.org/10.1063/1.4905840

Sachs, E., Cima, M., Cornie, J., n.d. Three-Dimensional Printing: Rapid Tooling and Prototypes Directly from a CAD Model 4.

Sachs, E., Wylonis, E., Allen, S., Cima, M., Guo, H., 2000. Production of injection molding tooling with conformal cooling channels using the three dimensional printing process. Polym. Eng. Sci. 40, 1232–1247. https://doi.org/10.1002/pen.11251

Sirringhaus, H., Kawase, T., Friend, R.H., Shimoda, T., Inbasekaran, M., Wu, W., Woo, E.P., 2000. High-Resolution Inkjet Printing of All-Polymer Transistor Circuits. Science 290, 2123–2126. https://doi.org/10.1126/science.290.5499.2123

Zhu, W., Li, J., Leong, Y.J., Rozen, I., Qu, X., Dong, R., Wu, Z., Gao, W., Chung, P.H., Wang, J., Chen, S., 2015. 3D-Printed Artificial Microfish. Adv. Mater. 27, 4411–4417. https://doi.org/10.1002/adma.201501372

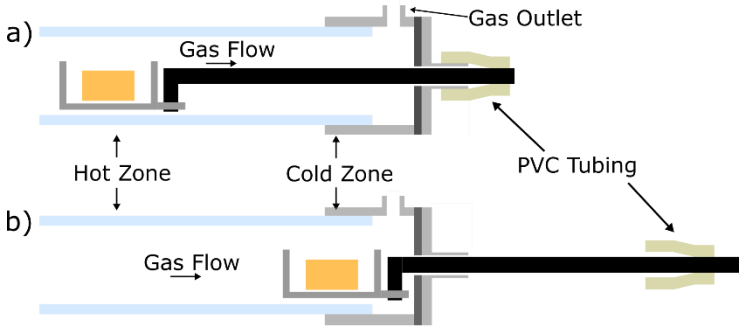
Ziaee, M., Crane, N.B., 2019. Binder jetting: A review of process, materials, and methods. Addit. Manuf. 28, 781–801. https://doi.org/10.1016/j.addma.2019.05.031

## Acknowledgments

I would like to acknowledge Brigham Young University College of Physical and Mathematical Sciences for operational funds and for Undergraduate Mentorship Funding. I would also like to acknowledge all of the help and mentoring from my research advisors, especially Dr. Davis and Dr. Vanfleet. Additionally, I would like to acknowledge the other students on the project.

# Supplementary Material

## Furnace Setup:




*Supplemental Figure 1: Furnace setup for sintering and infiltration. a) During sintering and infiltration, samples are inserted into the heating zone and the transfer arm is sealed with PVC tubing using hose clamps to minimize oxygen diffusion into furnace. b) After sintering or infiltration, samples are rapidly cooled by unsealing the transfer arm and pulling them out to the cooling zone.*

## Additional Samples from Pore Filling Study:




*Supplemental Figure 2: Images of all samples from pore filling study.*